Differentiation of Schizophrenia by Combining the Spatial EEG Brain Network Patterns of Rest and Task P300

Article *in* IEEE Transactions on Neural Systems and Rehabilitation Engineering · February 2019

DOI: 10.1109/TNSRE.2019.2900725

CITATIONS
12

READS
236

11 authors, including:

Fali Li
University of Electronic Science and Technology of China
61 PUBLICATIONS **708** CITATIONS
SEE PROFILE

Jiuju Wang
Peking University
21 PUBLICATIONS **158** CITATIONS
SEE PROFILE

Yajing Si
23 PUBLICATIONS **139** CITATIONS
SEE PROFILE

Wenjing Peng
Texas Tech University
34 PUBLICATIONS **329** CITATIONS
SEE PROFILE

Differentiation of Schizophrenia by Combining the Spatial EEG Brain Network Patterns of Rest and Task P300

Fali Li, Jiuju Wang, Yuanyuan Liao, Chanlin Yi, Yuanling Jiang, Yajing Si, Wenjing Peng, Dezhong Yao, Yangsong Zhang, Wentian Dong, and Peng Xu

***Abstract*— The P300 is regarded as a psychosis endophenotype of schizophrenia and a putative biomarker of risk for schizophrenia. However, the brain activity (i.e., P300 amplitude) during tasks cannot always provide satisfying discrimination of patients with schizophrenia (SZs) from healthy controls (HCs). Spontaneous activity at rest indices the potential of the brain, such that if the task information can be efficiently processed, it provides a compensatory understanding of the cognitive deficits in SZs. In this paper, based on the resting and P300 task electroencephalogram (EEG) data sets, we constructed functional EEG networks and then extracted the inherent spatial pattern of network (SPN) features for both brain states. Finally, the combined SPN features of the rest and task networks were used to recognize SZs. The findings of this paper revealed that the combined SPN features could achieve the highest accuracy of 90.48%, with the sensitivity of 89.47%, and specificity of 91.30%. These findings consistently implied that the rest and task P300 EEGs could actually provide comprehensive information to reliably classify SZs from HCs, and the SPN is a promising tool for the clinical diagnosis of SZs.**

Manuscript received August 21, 2018; revised November 23, 2018 and January 24, 2019; accepted February 18, 2019. Date of publication February 22, 2019; date of current version April 8, 2019. This work was supported in part by the National Natural Science Foundation of China under Grant 61522105, Grant 61603344, Grant 81330032, Grant 71601136, and Grant 81771925, in part by the Open Foundation of Henan Key Laboratory of Brain Science and Brain-Computer Interface Technology under Grant HNBBL17001, in part by the Longshan Academic Talent Research Supporting Program of the Southwest University of Science and Technology under Grant 17LZX692, and in part by the Chengdu's HuiMin Projects of Science and Technology in 2013. *(Fali Li, Jiuju Wang, and Yuanyuan Liao contributed equally to this work.)* *(Corresponding authors: Wentian Dong; Peng Xu.)*

F. Li, Y. Liao, C. Yi, Y. Jiang, Y. Si, and W. Peng are with The Clinical Hospital of Chengdu Brain Science Institute, MOE Key Lab for Neuroinformation, University of Electronic Science and Technology of China, Chengdu 611731, China.

J. Wang and W. Dong are with the Institute of Mental Health, Peking University Sixth Hospital, National Clinical Research Center for Mental Disorders & Key Laboratory of Mental Health, Ministry of Health, Peking University, Beijing 100191, China (e-mail: dongwentian@bjmu.edu.cn).

D. Yao and P. Xu are with The Clinical Hospital of Chengdu Brain Science Institute, MOE Key Lab for Neuroinformation, University of Electronic Science and Technology of China, Chengdu 611731, China, and also with the School of Life Science and Technology, Center for Information in Medicine, University of Electronic Science and Technology of China, Chengdu 611731, China (e-mail: xupeng@uestc.edu.cn).

Y. Zhang is with The Clinical Hospital of Chengdu Brain Science Institute, MOE Key Lab for Neuroinformation, University of Electronic Science and Technology of China, Chengdu 611731, China, and also with the School of Computer Science and Technology, Southwest University of Science and Technology, Mianyang 621010, China.

Digital Object Identifier 10.1109/TNSRE.2019.2900725

***Index Terms*— Classification, functional brain network, P300, spatial pattern of network, schizophrenia.**

I. Introduction

SCHIZOPHRENIA refers to the cognitive disturbance in patients in identifying, processing, and responding to salient or novel stimuli [1]. Previous studies have demonstrated that patients with schizophrenia (SZs) exhibit comparable abnormalities in cognitive function, including attention and working memory, compared to healthy controls (HCs) [2]–[4]. Related studies also showed dysfunctions in certain regions, such as the anterior cingulate cortex and prefrontal cortex (PFC), in SZs [5]–[7]. For example, in multiple regions, including the thalamus and PFC, reduced gray matter volume was found in SZs [8]. In fact, these abnormalities are interpreted as disturbed neural connectivity that is called the "disconnectivity hypothesis" [9], [10].

The P300 can be evoked by a target stimulus during a task [11] and is characterized by the largest positive peak at approximately 300 ms after target onset and prominently over the parietal scalp region. The P300 is widely used in multiple studies related to cognition [12]–[14], neuropsychiatric disorders [15], and brain-computer interfaces [16]–[19]. Specifically, the P300 is regarded as an endophenotype of schizophrenia [20], [21]. The P300 can thereby be used to index neurobiological vulnerability to schizophrenia, and also to evaluate the cognitive capacity of patients [22], [23]. In essence, a target stimulus can evoke a clear P300 only if the related information is efficiently processed in the brain, which is attributed to the effective allocation of related resources [24], [25]. Dysfunction of these regions leads to P300 deficits, including decreased amplitude and prolonged latency [26], [27]. Herein, investigating P300 variability between patients and controls helps to deepen our knowledge of the cognitive deficits in SZs and to differentiate SZs from HCs [28]–[30]. For example, using multiple P300 variables (e.g., four amplitude and three latency), Chun and colleagues obtained 83% classification accuracy when recognizing SZs [31]. A similar study provided a positive prediction of 72.73% and a negative prediction of 78.95% when the Kullback-Leibler divergence and relative power of multiple P300 trials were used [32].

When the brain is at rest, the spontaneous activity may reflect the potential of the brain to efficiently process

task information [33]–[35]. Resting brain activity can, therefore, be used to study the pathophysiological mechanism of brain disease and to classify patients [36]–[38]. The brain functions as a large-scale complex network [39]. In the brain, information is processed within spatially distributed but functionally coupled regions [40]–[42]. Methods including coherence [43] and phase locking value (PLV) [44]–[46] can be used to construct the brain network for both rest and task electroencephalograms (EEGs). A high accuracy of approximately 90% was achieved using two rest EEG network measurements to classify amnestic mild cognitive impairment from normal cognition [47]. Schizophrenia is attributed to disconnectivity in brain architecture and to evaluate variations between patients and controls, multiple network measurements can be extracted and then used to categorize these two groups. For example, Gomez-Pilar and colleagues calculated the Shannon Graph Complexity of the corresponding network that was used to recognize SZs, which achieved an accuracy of 72.5% [48]. The relatively low accuracy might be due to this feature being a direct statistical measure of a network and cannot encompass the entire spatial information related to network topologies.

The Spatial Pattern of Network (SPN) is an extension of common spatial pattern to the spatial network topology. The SPN uses a supervised learning approach to extract the differential network structure by emphasizing the important network nodes with larger coefficients while suppressing other less important nodes with smaller coefficients. The "disconnectivity" in the brain architecture is demonstrated for SZs [49], and the SPN is thus helpful for capturing the network topological differences between patients and controls that annot be uncovered by other properties. For example, based on the resting EEG network, our previous study used network topology to discriminate psychogenic nonepileptic seizures from epilepsy patients, which had 92% accuracy [37].

Since various studies demonstrated that the long duration of mental abnormalities can be reflected by both rest and task brain networks in schizophrenia [7], [9], [23], the functional networks of both rest and task states may reflect the different aspects of brain deficits in schizophrenia. The EEG features derived from two separate brain states might also provide comprehensive information for discrimination. In this work, motivated by the physiological basis that resting and task P300 EEGs reflect different aspects of the brain, we first collected the resting-state and task P300 EEG data sets. Then, based on the constructed resting and task EEG networks, we used the SPN to extract the combined spatial patterns of networks at rest and during a task, aiming to utilize the comprehensive information from both brain states to discriminate SZs from HCs.

II. Methods

A. Participants

This study was approved by the Peking University Sixth Hospital Ethics Committee. All participants received details about the experiment and were required to read and sign their name on written informed consents before participating.

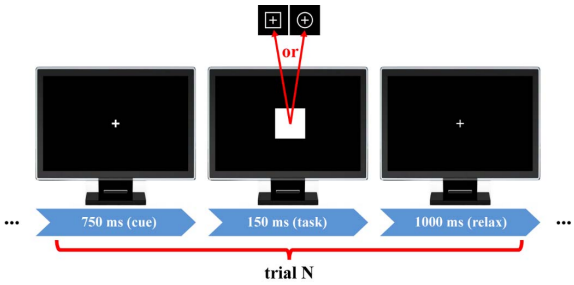

Fig. 1. Experimental protocol of the visual P300 task. A 750-ms cue, 150-ms stimulus, and 1000-ms break were included in each P300 trial. The squares and circles with a thin cross in the center were defined as the standard and target stimuli, respectively.

Forty-eight right-handed (self-reported) subjects, including twenty-three SZs (10 females, age 28.87 ± 7.68) and twenty-five HCs (11 females, age 29.44 ± 5.75), participated in this study. All subjects had normal or corrected-to-normal visual acuity. None of them had histories of substance abuse, took medication with deleterious effects on cognition, and had neurological illness. Since there were not enough trials left in their rest or task data sets after preprocessing, six subjects (four SZs and two HCs) were excluded from further analysis. Therefore, nineteen SZs and twenty-three HCs were included in the following study.

B. Experimental Procedures

Before the experiments, all subjects were seated comfortably, stayed relaxed and were required to control their body movements and eye blinks during the experiments. In this study, a square with a thin cross in the center was defined as the standard stimulus, and a circle with a thin cross in the center was defined as the target stimulus. During experiments, a five-minute, eye-closed resting-state session and four runs of P300 tasks were included. Between two adjacent recording stages, a 4-min break was set. Within each P300 run, a total of 100 stimuli, 80 standards and 20 targets, were randomly presented on the computer screen. Within each P300 trial (Fig. 1), subjects were asked to fixate on the center of the screen, and a bold-cross cue was first presented and lasted 750 ms to warn subjects to focus their attention and to inform them that a standard (or target) stimulus would appear very soon. A standard (or target) stimulus then appeared on the screen for 150 ms. At the same time, subjects pressed the '1' key on a standard keyboard when they saw a target stimulus. After a 1000-ms break, the next trial initiated.

C. EEG Data Acquisition

Resting and task EEG data sets were recorded using the Symtop amplifier (Symtop Instrument, Beijing, China) and a 16-channel Ag/AgCl (i.e., Fp1, Fp2, F3, F4, C3, C4, P3, P4, O1, O2, F7, F8, T3, T4, T5, and T6) electrode cap (BrainMaster, Inc., Shenzhen, China). All electrodes were positioned in compliance with the 10–20 international electrode placement system. During online data recording, electrode AFz served as the reference. EEG signals were sampled at 1000 Hz and online bandpass filtered at 0.05-100 Hz. During recording, the impedances of all electrodes were kept below 5 KΩ.

D. EEG Data Analysis

1) Data Pre-Processing: Multiple procedures, including Reference Electrode Standardization Technique (REST) referencing [50]–[52], [0.5 Hz, 30 Hz] offline bandpass filtering 1-s length data segmenting (between 200 ms before and 800 ms after targets onset, [−200 ms, 800 ms]), [−200 ms, 0 ms] baseline correction, and artifact-trial removal using a threshold of ±100 μv, were used to preprocess the task data sets.

For rest data sets, the following preprocessing procedures were used: REST referencing, [0.5 Hz, 30 Hz] offline-bandpass filtering, the first and last ten seconds in EEG signals were excluded, and the remaining portion was segmented into 1-s length rest segments. Then, a threshold of ±100 μv was also used to automatically exclude segments with absolute magnitudes exceeding 100 μv in any recorded channel.

2) P300 Amplitude: All artifact-free task P300 trials were trial-averaged for each subject. Based on the averaged P300 ERP, P300 amplitudes of electrodes C3, C4, P3, and P4 were defined as its highest peak within a time window of [300, 500] ms. Then, the underlying differences in P300 amplitudes between SZs and HCs were investigated using independent t-tests.

3) Brain Networks: The PLV can be used to estimate the phase-synchronization among each pair of electrodes [45], [53], and the corresponding PLV value is defined within the range of [0, 1]. Higher values represent the stronger strength of phase-synchronization.

To estimate the corresponding instantaneous phases, $\phi_x(t)$ and $\phi_y(t)$, of two given time series, $x(t)$ and $y(t)$, the Hilbert transform (HT) is used to form the analytical signal $H(t)$ as follows:

$$\begin{cases} H_x(t) = x(t) + iHT_x(t) \\ H_y(t) = y(t) + iHT_y(t) \end{cases} \tag{1}$$

where $HT_x(t)$ and $HT_y(t)$ are the HT of these two time series, $x(t)$ and $y(t)$, which are defined as follows:

$$\begin{cases} HT_x(t) = \dfrac{1}{\pi} P.V. \displaystyle\int_{-\infty}^{\infty} \dfrac{x(t')}{t-t'} dt' \\ HT_y(t) = \dfrac{1}{\pi} P.V. \displaystyle\int_{-\infty}^{\infty} \dfrac{y(t')}{t-t'} dt' \end{cases} \tag{2}$$

where the $P.V.$ denotes the Cauchy principal value. Afterward, the corresponding analytical signal phases, $\phi_x(t)$ and $\phi_y(t)$, can be computed as follows:

$$\begin{cases} \phi_x = arctan \dfrac{HT_x(t)}{x(t)} \\ \phi_y = arctan \dfrac{HT_y(t)}{y(t)} \end{cases} \tag{3}$$

Finally, the PLV is formulated as follows:

$$w^{plv} = \left| \frac{1}{N} \sum_{j=0}^{N-1} e^{i(\phi_x(j\Delta t) - \phi_y(j\Delta t))} \right| \tag{4}$$

where w^{plv} is the connection weight estimated by PLV, Δt is the sampling period, and N denotes the sample number.

In this study, the PLV was used to estimate the adjacency matrix per rest segment (also task trial) per subject. Afterward, for each subject, the final weighted rest (also task) brain network, a 16 × 16 adjacency matrix, was acquired by averaging matrices across all artifact-free rest segments (also task trials). Based on these EEG networks of both rest and task brain states, independent t-tests were used to uncover potential differences in brain architectures between the two groups.

4) Network Properties: To quantitatively measure the efficiency of the brain when processing related information, in this study, four weighted network properties, namely, clustering coefficient (C), characteristic path length (L), global efficiency (Ge), and local efficiency (Le), were calculated. Here, d_{ij} represents the shortest weighted path length between nodes i and j, n represents the node number, and Ψ represents the set of nodes in a given network. These four network properties were formulated as follows:

$$C = \frac{1}{n} \sum_{i \in \Psi} \frac{\sum_{j,h \in \Psi} \left(w_{ij}^{plv} w_{ih}^{plv} w_{jh}^{plv} \right)^{1/3}}{\sum_{j \in \Psi} w_{ij}^{plv} \left(\sum_{j \in \Psi} w_{ij}^{plv} - 1 \right)} \tag{5}$$

$$L = \frac{1}{n} \sum_{i \in \Psi} \frac{\sum_{j \in \Psi, j \neq i} d_{ij}}{n-1} \tag{6}$$

$$Ge = \frac{1}{n} \sum_{i \in \Psi} \frac{\sum_{j \in \Psi, j \neq i} \left(d_{ij} \right)^{-1}}{n-1} \tag{7}$$

$$Le = \frac{1}{n} \sum_{i \in \Psi} \frac{\sum_{j,h \in \Psi, j \neq i} \left(w_{ij}^{plv} w_{ih}^{plv} \left[d_{jh}(\Psi_i) \right]^{-1} \right)^{1/3}}{\sum_{j \in \Psi} w_{ij}^{plv} \left(\sum_{j \in \Psi} w_{ij}^{plv} - 1 \right)} \tag{8}$$

In this study, we used the brain connectivity toolbox (BCT, http://www.nitrc.org/projects/bct/) to calculate these four weighted network properties for both rest and task networks. Thereafter, we statistically compared these weighted network properties between SZs and HCs using independent t-tests to investigate differences between groups.

5) Spatial Patterns of Brain Networks: The network property is the statistical measure of the brain network and cannot encompass all information contained in the network topology. To extract the discriminative spatial pattern contained in a given brain network, we used the SPN approach developed in our previous work [37]. Let M_1 and M_2 represent the adjacency matrix of HCs and SZs in training set estimated by PLV, respectively, which contained spatial network patterns differentiated between two groups. Particularly, M_1 and M_2 were calculated by averaging the adjacency matrices of all subjects in HCs and SZs of the training set, respectively. In essence, the SPN filter is the projection derived by maximizing the generalized Rayleigh quotient $F(z)$, which can be formulated in (9) as follows:

$$\arg_z \max F(z) = \frac{(zM_1)(zM_1)^T}{(zM_2)(zM_2)^T} = \frac{zM_1M_1^Tz^T}{zM_2M_2^Tz^T} = \frac{z\Theta_1 z^T}{z\Theta_2 z^T} \tag{9}$$

where Θ_1 and Θ_2 are the covariance matrices of M_1 and M_2 for HCs and SZs, respectively.

Since the scaling of projection z has no effect on the object value, (9) can be rewritten as a constrained optimization problem as follows:

$$\begin{cases} \arg\max\limits_{z} \; z\Theta_1 z^T \\ subject\ to\ z\Theta_2 z^T = 1 \end{cases} \tag{10}$$

which can be further rewritten as (11) by introducing the Lagrange multiplier as follows:

$$L(z, \lambda) = z\Theta_1 z^T - \lambda\left(z\Theta_2 z^T - 1\right) \tag{11}$$

Then, under the condition $\frac{\partial L}{\partial z} = 0$, the objective projection z can be estimated using the generalized eigenvalue equation by taking the derivative of (11) with respect to z as follows:

$$\Theta_1 z^T = \lambda\Theta_2 z^T \tag{12}$$

where λ denotes the eigenvalue of generalized eigenvalue equation, and z is the eigenvector [54].

For multiple m SPN filters, (12) can be solved as follows:

$$\Theta_2^{-1}\Theta_1 Z^T = \sum Z^T \tag{13}$$

where Z consists of the eigenvectors of $\Theta_2^{-1}\Theta_1$ and $\sum = diag(\lambda_1, \lambda_2, \ldots, \lambda_m)$ with λ being the singular values. In the SPN, differentiation abilities of m SPN filters are represented by the eigenvalues involved in Σ[55].

In this study, different numbers of SPN filters were used to extract the SPN features. Taking 2 pairs of SPN filters as an example, 4-dimensional SPN features are acquired during this process [54], [56]. Theoretically, 2 pairs of SPN filters (i.e., 4 SPN filters) comprise a matrix $V_{SPN} = [z_1, z_2, z_3, z_4]$. For a 16×16 adjacency matrix, M, each SPN filter is a 16-length vector and therefore V_{SPN} is 16×4. Eventually, by calculating the variance of each row of the weighted nodes, the corresponding SPN features were given as a vector with a length of 4 and were calculated as follows:

$$F_{SPN} = log(var(V_{SPN}^T M)) \tag{14}$$

where $var(\cdot)$ denotes the variance operation for each row of the SPN transformed matrix.

In this study, after these ERP (i.e., P300 amplitudes) and network features (i.e., weighted network properties and SPN features) were defined and extracted, we performed the classification analysis between SZs and HCs using these features. Moreover, to obtain good performance, we considered two different strategies, namely, discriminating SZs and HCs using the ERP and network features in separate brain states and using the combined network features in rest and task states.

6) Discrimination of SZs From HCs Based on ERP and Network Features in Separate Brain States: The corresponding ERP and network features either at rest or in a task state in training data sets were separately used in the training process. For the SPN features, based on the constructed 16×16 adjacency matrices of rest and task states, the SPN filters were calculated according to the above procedures [(9)–(14)]. The estimated SPN filters were then applied to training sets to extract the corresponding SPN features for rest or task EEGs. For the network property features, the weighted network properties (i.e., C, L, Ge, and Le) can be calculated for either the rest or task state using the definitions in (5)–(8). For the ERP features, P300 amplitudes of training sets were calculated following the descriptions in D.2. Afterward, based on those features in separate brain states (i.e., either rest or task), linear discriminant analysis (LDA) and support vector machine (SVM) with radial basis kernel were trained by the training features. For SVM, in this study, a grid search approach was applied to search for the optimized parameters in the training process [57].

In the recognition process, the SPN filters estimated in the training process were then used to extract spatial network topology information (i.e., SPN features) from the adjacency matrix of test sets. The corresponding P300 amplitudes and weighted network properties of test sets were also calculated for either the rest or task state. Finally, based on these EEG features (i.e., P300 amplitudes, network properties, and SPN features), the trained LDA/SVM classifiers were adopted to differentiate the SZs and HCs, resulting in the corresponding classification accuracies for rest or task EEGs.

7) Discrimination Based on the Combined Network Features of Rest and Task States: Considering that rest and task EEGs reflect different aspects of the brain, the features derived from two separate states might provide comprehensive information for discrimination. In this study, we further proposed combining the network features of the two brain states together to discriminate SZs. The network properties (also SPN features) of both rest and task states were concatenated together to form the new network features.

In the current work, we adopted similar procedures to create the states fusions of different network features. For the state fusion of network properties, the network properties of rest and task EEGs were concatenated together to form a new feature for the training and testing. For the fusion of SPN features, similarly, the corresponding SPN features from the two states were also concatenated to generate newly combined SPN features for training and testing. Then, based on newly generated features, the training and testing procedures were performed for the recognition between SZs and HCs. Fig. 2 gives detailed procedures for the combination of SPN features. Specifically, the procedures in Fig. 2 consisted of training and testing subprocedures. The training subprocedure generated the corresponding SPN filters for rest and task EEGs and the corresponding rest and task SPN features, which were then concatenated together to form the new training features. After the training subprocedure, the SPN filters were further applied to the testing sets to extract the corresponding SPN features for rest and task EEGs. These test SPN features were also concatenated together to form new testing features. In the state fusion classification, the combined training features were used to train the LDA/SVM classifier model, and the combined SPN features derived from the testing set were finally fed into the trained classifier model for the recognition of SZs.

8) Evaluation Indices: Considering that the present dataset is relatively small, the leave-one-out cross-validation (LOOCV)

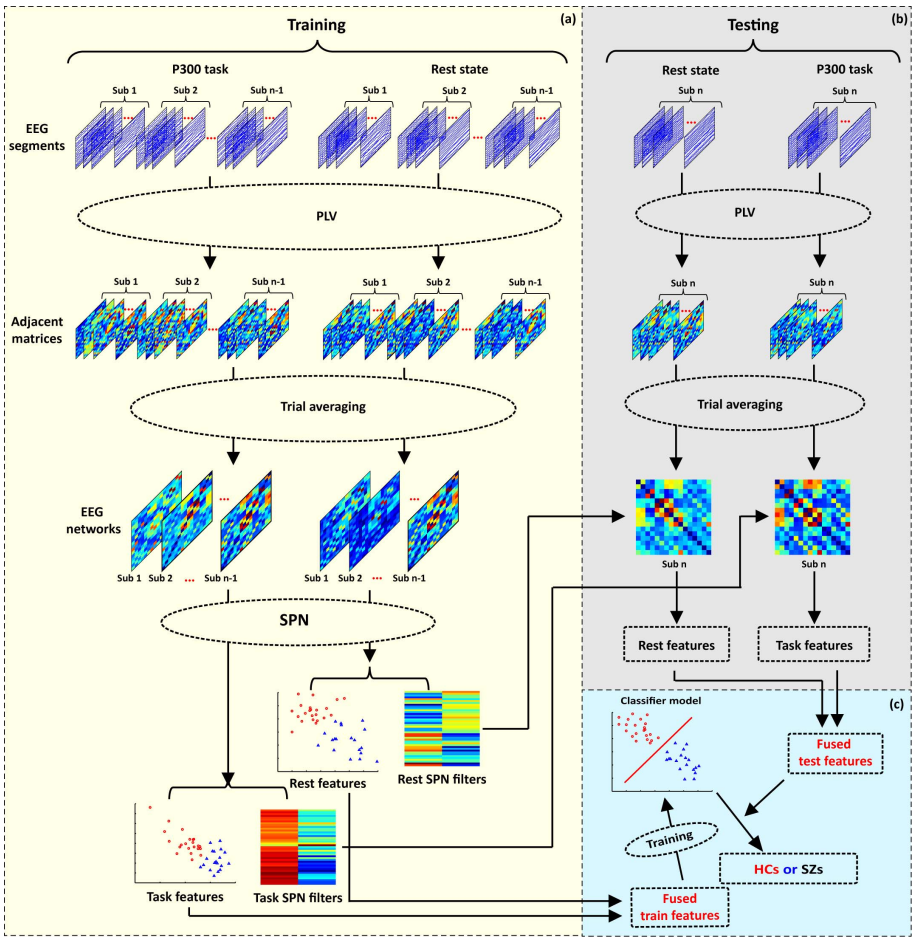

Fig. 2. The procedures for the fusion of SPN features between rest and task EEGs. (a) Training feature extraction, (b) Test feature extraction, and (c) State fusion classification.

test was used to recognize SZs [58], [59]. Based on the LOOCV, three indices including accuracy (*ACC*), sensitivity (*SEN*), and specificity (*SPE*) were then used to evaluate the classification performance. Let N_{SZs} and N_{HCs} denote the total number of SZs and HCs, respectively, n_{SZs} and n_{HCs} denote the correctly discriminated number of SZs and HCs, respectively. The detailed calculations of these three indices were formulated as follows:

$$ACC = \frac{n_{SZs} + n_{HCs}}{N_{SZs} + N_{HCs}} \times 100\% \quad (15)$$

$$SEN = \frac{n_{SZs}}{N_{SZs}} \times 100\% \quad (16)$$

$$SPE = \frac{n_{HCs}}{N_{HCs}} \times 100\% \quad (17)$$

III. Results

A. P300 of HCs and SZs

In our study, to visually show the differences between the HCs and SZs, Fig. 3 provides the evoked P300 waveforms at four electrodes (i.e., C3, C4, P3, and P4) for both HCs and SZs. In Fig. 3, higher P300 peaks were found for HCs than SZs. The colored bars embedded in each subfigure quantitatively demonstrated the same trend in P300 amplitude between the two groups because the P300 amplitude of HCs was significantly ($p < 0.05$) larger than that of SZs.

B. Brain Networks Between HCs and SZs

Fig. 4 demonstrates the significantly different ($p < 0.05$) network topologies between HCs and SZs for both rest and task brain states, where red indicates weaker linkages and blue indicates stronger linkages. In detail, when the brain is at rest, the EEG-based default mode network (DMN) shows stronger activity in SZs compared to HCs. During the task, the dominated stronger linkages among those multiple brain areas mainly located at frontal and parietal lobes were found for HCs compared to SZs.

We quantitatively measured the corresponding network efficiency by four measurements (*C*, *L*, *Ge*, and *Le*), as well as the underlying differences between HCs and SZs in both rest and task conditions. Although significant differences in network topology between the two groups are illustrated in Fig. 4, but no significant differences ($p > 0.05$) in weighted network properties were found.

C. Differentiated SPN Filters

Although obvious differences in topologies were observed between SZs and HCs at rest and in the P300 task,

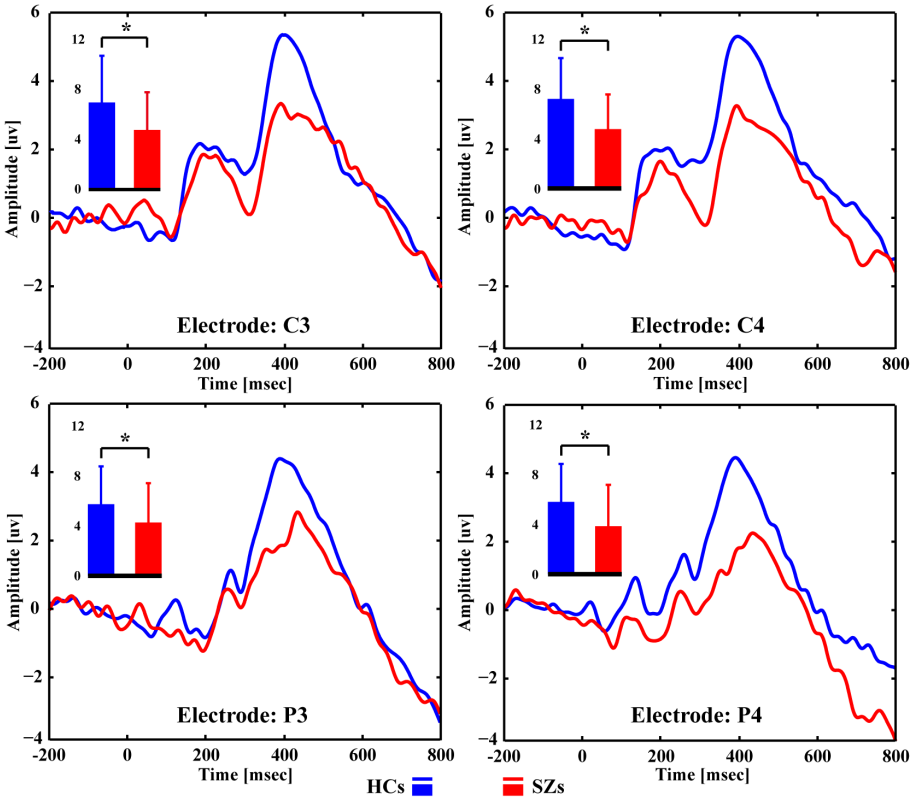

Fig. 3. P300 waveforms at multiple electrodes between HCs and SZs. In each subfigure, the blue and red solid lines denote the P300 waveforms of HCs and SZs, respectively, and the blue and red colored bars denote the corresponding P300 amplitudes of HCs and SZs, respectively.

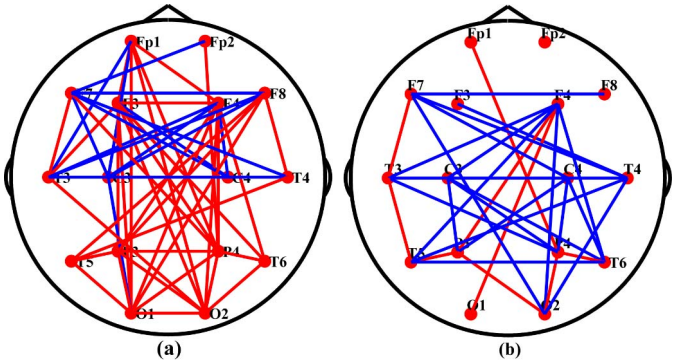

Fig. 4. Differentiated brain topology between HCs and SZs in the resting and task states. (a) Resting-state; (b) Task-state. In each subfigure, the red solid lines denote the weaker linkages of HCs compared to SZs, and the blue solid lines denote stronger linkages in HCs than SZs.

the network properties between these two groups were not statistically different. Therefore, we used the SPN to extract the implicit and inherent spatial network topologies to classify SZs and HCs. The most discriminative pair of SPN filters in Fig. 5 further demonstrated that the network nodes that had significant linkage differences in Fig. 4 were emphasized with larger coefficients (i.e., marked with deep red or blue colors), which was indeed useful for extracting discriminative spatial network patterns from Fig. 4.

D. Categorization into HCs and SZs

Based on the P300 amplitudes, network properties, and SPN patterns, we examined discrimination of SZs from HCs. The results are given in Table I. Among these three types of features, Table I consistently demonstrates that regardless of using separate or fused features to recognize SZs, the highest recognition performance was achieved for SPN features. Separate SPN features achieved 88.10% accuracy for both rest and task conditions, and combined SPN features at rest and in the task further improved accuracy to 90.48%.

IV. Discussion

The P300 reflects the relative amount of brain resources allocated to processing target information [13] and is affected by the effort and attention of individuals devoted to the P300 task. However, compared to the HCs, the SZs showed abnormalities in multiple cognitive functions, such as attention and working memory [22], [23], as well as the evoked P300 components [60], [61]. The SZs hardly sustained their attention as consistently as the HCs during tasks [62], and even for those trials in which the P300 was elicited, the P300 still fell below the normal level. This finding was also clarified by our results in Fig. 3, which show the smaller P300 components with the lower peaks in SZs. In our current study, when the P300 amplitude was adopted to classify SZs from HCs, Table I showed relatively low accuracy

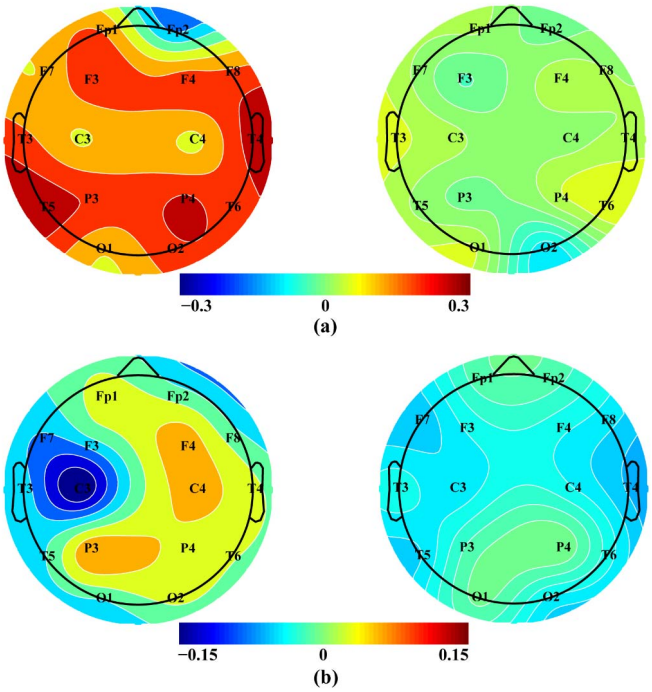

Fig. 5. The topological distribution of the most discriminative first pair of SPN filters between HCs and SZs in rest and task brain states. (a) Rest brain state, (b) Task brain state. The subfigures in the left and right columns denote the corresponding SPN Filters 1 and 2, respectively.

of 76.19% with 68.42% sensitivity and 82.61% specificity. Although the deficits in the P300 are robust findings widely reported in schizophrenia, the P300 amplitude could not always provide satisfying classification performance in identifying SZs from HCs. We assumed that this reduced ability might be attributed to the huge variability in P300 across individuals [63], [64].

Our brain works as a large-scale network, and efficient brain architecture, which contains multiple brain regions, supports the effortful P300 components (e.g., larger P300 amplitude) [27], [64], [65], whereas dysfunctions in related regions disturbed the brain's efficient processing of related information, which then led to the P300 deficits [27]. In addition to the task network, when subjects suffered from schizophrenia, the brain at rest was also reshaped by this abnormality [49]. Moreover, various studies have demonstrated that the brain will reconfigure the network architecture from a resting state to process task information [66]–[68]. Therefore, the task P300 and rest networks may reflect different aspects of abnormality in schizophrenia. The differential network topology in Fig. 4 consistently revealed dysfunctions in multiple regions in the brain for both rest and task P300s in SZs compared to HCs. In detail, at rest, much stronger DMN-like linkages were observed for SZs, whereas during the P300 task, decreased couplings among regions, such as the frontal and parietal lobes, were found in SZs. As illustrated [69]–[71], paranoid schizophrenics demonstrated increased sensitivity to both the external environment and self-referential or introspective thought. Their brains were more activated than HCs, even at rest, which resulted in increased functional connectivity within the DMN in SZs. However, during the following P300 task, due to the deficits in cognition, the decreased linkages within regions related to the P300 were then exhibited, such as in Fig. 4. In our present study, we assumed that the dysfunctions in related regions and their interactions failed to guarantee the brain's efficient processing of target information, which resulted in the cognitive deficits seen in SZs. To measure brain efficiency during the P300 task or at rest, the related network properties were calculated. However, these network properties, although essentially derived from the corresponding brain networks, still missed important spatial information, thereby failing to capture the distinct differences in network topologies in Fig. 4. No differences in network properties between the two groups were found in our present work either at rest or in the P300 task. This finding might account for the low accuracy when the network properties were used to differentiate the SZs as shown in Table I.

Due to the obvious topological differences revealed in Fig. 4 between these two groups, when the SPN features that reflected this difference were used, the related recognition achieved the highest accuracy among the three different features, as shown in Table I. As demonstrated, the SPN used a supervised learning approach to extract the differential network structure by emphasizing important network nodes with larger coefficients and suppressing less important nodes with smaller coefficients. Combing the mostly differential SPN filters in Fig. 5 and the differential network topologies in Fig. 4, we found that the SPN filters both at rest and during a task captured the differences in network topology between SZs and HCs, which was achieved by emphasizing the network nodes exhibiting significant differences between the two groups with larger coefficients (deep red or blue colors) and suppressing those nodes without linkage differences with much smaller coefficients (close to zero).

There are different strategies adopted by the SPN for the important and less important network nodes that can guarantee effective extraction of the reliable network spatial patterns to classify the two groups, consistently resulting in the highest recognition performance when the SPN features were adopted in three conditions (resting state, P300 task, and both states together). Specifically, as shown in Table I, we revealed the following different aspects of the SPN for SZs classification: 1) the number of SPN filters influenced the recognition performance. For each brain state, though the recognition performance of the SPN varied with the number of SPN filters, the SPN consistently achieved relatively higher classification accuracy compared to the other two approaches regardless of how many pairs of SPN filters were used. Among the three state conditions, the highest classification accuracy was consistently acquired utilizing two pairs of SPN filters. 2). The combination of SPN features at rest and in the P300 task state increased recognition to 90.48% when the corresponding spatial information extracted using the two pairs of SPN filters was fused. This performance improvement was attributed to the compensative information on brain network topology demonstrated in Fig. 4 for the rest and P300 task states. In essence, various studies demonstrated that the long duration of mental abnormalities could be reflected by both rest and task brain networks, and the two brain networks might reflect

TABLE I
DIFFERENTIATING PERFORMANCE OF MULTIPLE MEASUREMENTS UNDER DIFFERENT BRAIN STATES

Brain state	Features	LDA			SVM		
		ACC(%)	SEN(%)	SPE(%)	ACC(%)	SEN(%)	SPE(%)
Task	Amplitude	52.38	57.89	47.83	76.19	68.42	82.61
	Network property	42.86	47.37	39.13	54.76	0.00	100.00
	SPN: One pair	61.90	68.42	56.52	73.81	57.89	86.96
	SPN: Two pairs	85.71	89.47	82.61	**88.10**	**84.21**	**91.30**
	SPN: Three pairs	83.33	89.47	78.26	85.71	84.21	86.96
Rest	Network property	71.43	63.16	78.26	54.76	0.00	100.00
	SPN: One pair	73.81	63.16	82.61	76.19	68.42	82.61
	SPN: Two pairs	83.33	73.68	91.30	**88.10**	**78.95**	**95.65**
	SPN: Three pairs	80.95	73.68	86.96	83.33	78.95	86.96
States fusion	Network property	64.29	57.89	69.57	54.76	0.00	100.00
	SPN: One pair	76.19	73.68	78.26	80.95	73.68	86.96
	SPN: Two pairs	85.71	78.95	91.30	**90.48**	**89.47**	**91.30**
	SPN: Three pairs	85.71	89.47	82.61	90.48	89.47	91.30

the different aspects of brain deficits in schizophrenia. Herein, the fusion of network topological information in the two brain states potentially differentiated SZs from HCs based on scalp EEG.

V. CONCLUSION

This study investigated the differentiable network topologies between SZs and HCs in both the rest and task brain states, as well as the evoked P300 amplitudes during a task. The spatial pattern of the EEG network extracted using the SPN had much better performance than common features in discriminating SZs from HCs, such as P300 amplitude and network properties. Moreover, the combination of SPN features in different brain states (i.e., rest and task) could reliably differentiate the two groups with an accuracy of 90.48%, a sensitivity of 89.47%, and a specificity of 91.30%.

REFERENCES

[1] T. R. Insel, "Rethinking schizophrenia," *Nature*, vol. 468, no. 7321, pp. 187–193, Nov. 2010.

[2] J. Smucny, A. Olincy, L. C. Eichman, E. Lyons, and J. R. Tregellas, "Early sensory processing deficits predict sensitivity to distraction in schizophrenia," *Schizophrenia Res.*, vol. 147, no. 1, pp. 196–200, Jun. 2013.

[3] T. Onitsuka, N. Oribe, I. Nakamura, and S. Kanba, "Review of neurophysiological findings in patients with schizophrenia," *Psychiatry Clin. Neurosci,*, vol. 67, no. 7, pp. 461–470, Nov. 2013.

[4] J. Prado, J. Carp, and D. H. Weissman, "Variations of response time in a selective attention task are linked to variations of functional connectivity in the attentional network," *NeuroImage*, vol. 54, no. 1, pp. 541–549, Jan. 2011.

[5] E. Mouchlianitis *et al.*, "Treatment-resistant schizophrenia patients show elevated anterior cingulate cortex glutamate compared to treatment-responsive," *Schizophrenia Bull.*, vol. 43, no. 3, pp. 744–752, May 2015.

[6] T. Ohtani *et al.*, "Abnormalities in white matter connections between orbitofrontal cortex and anterior cingulate cortex and their associations with negative symptoms in schizophrenia: A DTI study," *Schizophrenia Res.*, vol. 157, nos. 1–3, pp. 190–197, Aug. 2014.

[7] F. Li *et al.*, "Top-down disconnectivity in schizophrenia during P300 tasks," *Frontiers Comput. Neurosci.*, vol. 12, p. 33, May 2018.

[8] C. Schuster *et al.*, "Gray matter volume decreases in elderly patients with schizophrenia: A voxel-based morphometry study," *Schizophrenia Bull.*, vol. 38, no. 4, pp. 796–802, Jul. 2012.

[9] K. J. Friston and C. D. Frith, "Schizophrenia: A disconnection syndrome?" *Clin. Neurosci.*, vol. 3, no. 2, pp. 89–97, 1995.

[10] K. E. Stephan, K. J. Friston, and C. D. Frith, "Dysconnection in schizophrenia: From abnormal synaptic plasticity to failures of self-monitoring," *Schizophrenia Bull.*, vol. 35, no. 3, pp. 509–527, May 2009.

[11] N. K. Squires, K. C. Squires, and S. A. Hillyard, "Two varieties of long-latency positive waves evoked by unpredictable auditory stimuli in man," *Electroencephalogr. Clin. Neurophysiol.*, vol. 38, no. 4, pp. 387–401, Apr. 1975.

[12] D. E. J. Linden, "The P300: Where in the brain is it produced and what does it tell us?" *Neuroscientist*, vol. 11, no. 6, pp. 563–576, Dec. 2005.

[13] J. Polich, "Updating P300: An integrative theory of P3a and P3b," *Clin. Neurophysiol.*, vol. 118, no. 10, pp. 2128–2148, Oct. 2007.

[14] J. Polich and J. R. Criado, "Neuropsychology and neuropharmacology of P3a and P3b," *Int. J. Psychophysiol.*, vol. 60, no. 2, pp. 85–172, May 2006.

[15] V. Molina *et al.*, "Dorsolateral prefrontal cortex contribution to abnormalities of the P300 component of the event-related potential in schizophrenia," *Psychiatry Res., Neuroimag.*, vol. 140, no. 1, pp. 17–26, Oct. 2005.

[16] Y. Li *et al.*, "Multimodal BCIs: Target detection, multidimensional control, and awareness evaluation in patients with disorder of consciousness," *Proc. IEEE*, vol. 104, no. 2, pp. 332–352, Feb. 2016.

[17] Y. Li *et al.*, "An EEG-based BCI system for 2-D cursor control by combining mu/beta rhythm and P300 potential," *IEEE Trans. Biomed. Eng.*, vol. 57, no. 10, pp. 2495–2505, Oct. 2010.

[18] Y. Li, J. Pan, F. Wang, and Z. Yu, "A hybrid BCI system combining P300 and SSVEP and its application to wheelchair control," *IEEE Trans. Biomed. Eng.*, vol. 60, no. 11, pp. 3156–3166, Nov. 2013.

[19] J. Long, Y. Li, H. Wang, T. Yu, J. Pan, and F. Li, "A hybrid brain computer interface to control the direction and speed of a simulated or real wheelchair," *IEEE Trans. Neural Syst. Rehabil. Eng.*, vol. 20, no. 5, pp. 720–729, Sep. 2012.

[20] E. Bramon, S. Rabe-Hesketh, P. Sham, R. M. Murray, and S. Frangou, "Meta-analysis of the P300 and P50 waveforms in schizophrenia," *Schizophrenia Res.*, vol. 70, nos. 2–3, pp. 315–329, Oct. 2004.

[21] E. Bramon *et al.*, "Is the P300 wave an endophenotype for schizophrenia? A meta-analysis and a family study," *NeuroImage*, vol. 27, no. 4, pp. 960–968, Oct. 2005.

[22] A. J. Rissling, S. Makeig, D. L. Braff, and G. A. Light, "Neurophysiologic markers of abnormal brain activity in schizophrenia," *Current Psychiatry Rep.*, vol. 12, no. 6, pp. 572–578, Dec. 2010.

[23] D. I. Leitman, P. Sehatpour, B. A. Higgins, J. J. Foxe, G. Silipo, and D. C. Javitt, "Sensory deficits and distributed hierarchical dysfunction in schizophrenia," *Amer. J. Psychiatry*, vol. 167, no. 7, pp. 818–827, May 2010.

[24] F. Musso *et al.*, "Ketamine effects on brain function–simultaneous fMRI/EEG during a visual oddball task," *NeuroImage*, vol. 58, no. 2, pp. 508–525, Sep. 2011.

[25] C. Bledowski *et al.*, "Localizing P300 generators in visual target and distractor processing: A combined event-related potential and functional magnetic resonance imaging study," *J. Neurosci.*, vol. 24, no. 42, pp. 9353–9360, Oct. 2004.

[26] S. Yamaguchi and R. T. Knight, "Anterior and posterior association cortex contributions to the somatosensory P300," *J. Neurosci.*, vol. 11, no. 7, pp. 2039–2054, Jul. 1991.

[27] K. Daffner *et al.*, "Frontal and parietal components of a cerebral network mediating voluntary attention to novel events," *J. Cogn. Neurosci.*, vol. 15, no. 2, pp. 294–313, Feb. 2003.

[28] Y. W. Jeon and J. Polich, "Meta-analysis of P300 and schizophrenia: Patients, paradigms, and practical implications," *Psychophysiology*, vol. 40, no. 5, pp. 684–701, Sep. 2003.

[29] R. M. G. Reinhart, D. H. Mathalon, B. J. Roach, and J. M. Ford, "Relationships between pre-stimulus gamma power and subsequent P300 and reaction time break down in schizophrenia," *Int. J. Psychophysiol.*, vol. 79, no. 1, pp. 16–24, Jan. 2011.

[30] P. Fusar-Poli *et al.*, "White matter alterations related to P300 abnormalities in individuals at high risk for psychosis: An MRI-EEG study," *J. Psychiatry Neurosci.*, vol. 36, no. 4, pp. 239–248, Jul. 2011.

[31] J. Chun *et al.*, "Can P300 distinguish among schizophrenia, schizoaffective and bipolar I disorders? An ERP study of response inhibition," *Schizophrenia Res.*, vol. 151, nos. 1–3, pp. 175–184, Dec. 2013.

[32] P. Núñez *et al.*, "Exploring non-stationarity patterns in schizophrenia: Neural reorganization abnormalities in the alpha band," *J. Neural Eng.*, vol. 14, no. 4, Aug. 2017, Art. no. 046001.

[33] T. Zhang *et al.*, "Structural and functional correlates of motor imagery BCI performance: Insights from the patterns of fronto-parietal attention network," *NeuroImage*, vol. 134, pp. 475–485, Jul. 2016.

[34] R. Zhang *et al.*, "Efficient resting-state EEG network facilitates motor imagery performance," *J. Neural Eng.*, vol. 12, no. 6, Dec. 2015, Art. no. 066024.

[35] Y. Zhang, P. Xu, D. Guo, and D. Yao, "Prediction of SSVEP-based BCI performance by the resting-state EEG network," *J. Neural Eng.*, vol. 10, no. 6, Dec. 2013, Art. no. 066017.

[36] Z. Zhang *et al.*, "Altered functional–structural coupling of large-scale brain networks in idiopathic generalized epilepsy," *Brain*, vol. 134, no. 10, pp. 2912–2928, Oct. 2011.

[37] P. Xu *et al.*, "Differentiating between psychogenic nonepileptic seizures and epilepsy based on common spatial pattern of weighted EEG resting networks," *IEEE Trans. Biomed. Eng.*, vol. 61, no. 6, pp. 1747–1755, Jun. 2014.

[38] Y. Sun *et al.*, "Disrupted functional brain connectivity and its association to structural connectivity in amnestic mild cognitive impairment and Alzheimer's disease," *PLoS ONE*, vol. 9, no. 5, May 2014, Art. no. e96505.

[39] S. E. Petersen and O. Sporns, "Brain networks and cognitive architectures," *Neuron*, vol. 88, no. 1, pp. 207–219, Oct. 2015.

[40] F. Li *et al.*, "The time-varying networks in P300: A task-evoked EEG study," *IEEE Trans. Neural Syst. Rehabil. Eng.*, vol. 24, no. 7, pp. 725–733, Jul. 2016.

[41] F. Li *et al.*, "The dynamic brain networks of motor imagery: Time-varying causality analysis of scalp EEG," *Int. J. Neural Syst.*, vol. 29, no. 1, Apr. 2019, Art. no. 1850016.

[42] D. S. Bassett and O. Sporns, "Network neuroscience," *Nature Neurosci.*, vol. 20, no. 3, pp. 353–364, Feb. 2017.

[43] R. Srinivasan, W. R. Winter, J. Ding, and P. L. Nunez, "EEG and MEG coherence: Measures of functional connectivity at distinct spatial scales of neocortical dynamics," *J. Neurosci. Methods*, vol. 166, no. 1, pp. 41–52, Oct. 2007.

[44] J. Sun, X. Hong, and S. Tong, "Phase synchronization analysis of EEG signals: An evaluation based on surrogate tests," *IEEE Trans. Biomed. Eng.*, vol. 59, no. 8, pp. 2254–2263, Aug. 2012.

[45] V. Sakkalis, "Review of advanced techniques for the estimation of brain connectivity measured with EEG/MEG," *Comput. Biol. Med.*, vol. 41, no. 12, pp. 1110–1117, Dec. 2011.

[46] J. Sun and M. Small, "Unified framework for detecting phase synchronization in coupled time series," *Phys. Rev. E, Stat. Phys. Plasmas Fluids Relat. Interdiscip. Top.*, vol. 80, no. 4, Oct. 2009, Art. no. 046219.

[47] P. Xu *et al.*, "Recognizing mild cognitive impairment based on network connectivity analysis of resting EEG with zero reference," *Physiol. Meas.*, vol. 35, no. 7, pp. 1279–1298, Jul. 2014.

[48] J. Gomez-Pilar *et al.*, "Novel measure of the weigh distribution balance on the brain network: Graph complexity applied to schizophrenia," in *Proc. 38th Annu. Int. Conf. IEEE Eng. Med. Biol. Soc. (EMBC)*, Aug. 2016, pp. 700–703.

[49] J. Sun *et al.*, "Abnormal dynamics of EEG oscillations in schizophrenia patients on multiple time scales," *IEEE Trans. Biomed. Eng.*, vol. 61, no. 6, pp. 1756–1764, Jun. 2014.

[50] L. Dong *et al.*, "MATLAB toolboxes for reference electrode standardization technique (REST) of scalp EEG," *Frontiers Neurosci.*, vol. 11, p. 601, Oct. 2017.

[51] D. Yao, "A method to standardize a reference of scalp EEG recordings to a point at infinity," *Physiol. Meas.*, vol. 22, no. 4, p. 693, Oct. 2001.

[52] D. Yao, "Is the surface potential integral of a dipole in a volume conductor always zero? A cloud over the average reference of EEG and ERP," *Brain Topography*, vol. 30, no. 2, pp. 161–171, Mar. 2017.

[53] J. Sun, Z. Li, and S. Tong, "Inferring functional neural connectivity with phase synchronization analysis: A review of methodology," *Comput. Math. Methods Med.*, vol. 2012, Apr. 2012, Art. no. 239210.

[54] B. Blankertz, G. Dornhege, M. Krauledat, K.-R. Müller, and G. Curio, "The non-invasive Berlin Brain–computer interface: Fast acquisition of effective performance in untrained subjects," *NeuroImage*, vol. 37, no. 2, pp. 539–550, Aug. 2007.

[55] B. Blankertz, R. Tomioka, S. Lemm, M. Kawanabe, and K.-R. Müller, "Optimizing spatial filters for robust EEG single-trial analysis," *IEEE Signal Process. Mag.*, vol. 25, no. 1, pp. 41–56, Jan. 2008.

[56] P. Xu, P. Yang, X. Lei, and D. Yao, "An enhanced probabilistic LDA for multi-class brain computer interface," *PLoS ONE*, vol. 6, no. 1, Jan. 2011, Art. no. e14634.

[57] C. C. Chang and C. J. Lin, "LIBSVM: A library for support vector machines," *ACM Trans. Intell. Syst. Technol.*, vol. 2, no. 3, p. 27, Apr. 2011.

[58] P. Xu, M. Kasprowicz, M. Bergsneider, and X. Hu, "Improved noninvasive intracranial pressure assessment with nonlinear kernel regression," *IEEE Trans. Inf. Technol. Biomed.*, vol. 14, no. 4, pp. 971–978, Jul. 2010.

[59] L. Zeng *et al.*, "Identifying major depression using whole-brain functional connectivity: A multivariate pattern analysis," *Brain*, vol. 135, pp. 1498–1507, May 2012.

[60] B. I. Turetsky *et al.*, "the utility of P300 as a schizophrenia endophenotype and predictive biomarker: Clinical and socio-demographic modulators in COGS-2," *Schizophrenia Res.*, vol. 163, nos. 1–3, pp. 53–62, Apr. 2015.

[61] A. Díez *et al.*, "Abnormal frontoparietal synaptic gain mediating the P300 in patients with psychotic disorder and their unaffected relatives," *Hum. Brain Mapping*, vol. 38, no. 6, pp. 3262–3276, Jun. 2017.

[62] K. H. Nuechterlein and M. E. Dawson, "A heuristic vulnerability/stress model of schizophrenic episodes," *Schizophrenia Bull.*, vol. 10, no. 2, pp. 300–312, 1984.

[63] B. Ou, C. Wu, G. Zhao, and J. Wu, "P300 amplitude reflects individual differences of navigation performance in a driving task," *Int. J. Ind. Ergonom.*, vol. 42, no. 1, pp. 8–16, Jan. 2012.

[64] F. Li *et al.*, "Relationships between the resting-state network and the P3: Evidence from a scalp EEG study," *Sci. Rep.*, vol. 5, Oct. 2015, Art. no. 15129.

[65] E. Kirino, A. Belger, P. Goldman-Rakic, and G. McCarthy, "Prefrontal activation evoked by infrequent target and novel stimuli in a visual target detection task: An event-related functional magnetic resonance imaging study," *J. Neurosci.*, vol. 20, no. 17, pp. 6612–6618, Sep. 2000.

[66] F. Li *et al.*, "Brain network reconfiguration during motor imagery revealed by a large-scale network analysis of scalp EEG," *Brain Topography*, vol. 32, no. 2, pp. 304–314, Mar. 2019.

[67] T. Zhang *et al.*, "Reconfiguration patterns of large-scale brain networks in motor imagery," in *Brain Structure and Function*. Heidelberg, Germany: Springer, 2018.

[68] D. H. Schultz and M. W. Cole, "Higher intelligence is associated with less task-related brain network reconfiguration," *J. Neurosci.*, vol. 36, no. 33, pp. 8551–8561, Aug. 2016.

[69] S. J. Broyd, C. Demanuele, S. Debener, S. K. Helps, C. J. James, and E. J. S. Sonuga-Barke, "Default-mode brain dysfunction in mental disorders: A systematic review," *Neurosci. Biobehavioral Rev.*, vol. 33, no. 3, pp. 279–296, Mar. 2009.

[70] Y. Zhou *et al.*, "Functional disintegration in paranoid schizophrenia using resting-state fMRI," *Schizophrenia Res.*, vol. 97, nos. 1–3, pp. 194–205, Dec. 2007.

[71] D. Ongür *et al.*, "Default mode network abnormalities in bipolar disorder and schizophrenia," *Psychiatry Res.*, vol. 183, no. 1, pp. 59–68, Jul. 2010.